Reduced-Order Modelling of Moore-Greitzer PDEs using Sparse Regression

Yusuf Aydogdu, Thambirajah Ravichandran, Alyssa Novelia and N. Sri Namachchivaya
Department of Applied Mathematics, University of Waterloo, Waterloo, Ontario N2L 3G1, Canada

Summary. This paper develops a data-driven reduced-order model of the viscous Moore-Greitzer (MG) partial differential equations (PDEs) by threading together ideas from dimensionality reduction to sparse regression and compressed sensing. Numerical simulation of the infinite dimensional viscous MG system is reduced into low dimensional data using principal component analysis (PCA) and autoencoder neural networks based dimensionality reduction methods. Based on the observation that MG equations close to bifurcations have a sparse representation (normal forms) with respect to high-dimensional polynomial spaces, we use the Sparse Identification of Nonlinear Dynamics (SINDy) algorithm which uses a collection of all monomials as a sampling matrix and a sparse regression technique to recover a system of two sparse ordinary differential equations (ODEs) with cubic nonlinearities.

Introduction

This paper develops data-driven theory and algorithms to detect and mitigate stall compressor instability. The motivation is to produce a high-fidelity simulation of a jet engine compressor called the digital twin, which has the ability to monitor and diagnose complex systems to improve performance efficiency and utilization. Jet engine compressor models typically integrate a hierarchy of multi-physics and multi-fidelity models which are continually updated with data streams from the sensors. The model used to describe airflow inside the jet engine compressor is the viscous MG equations [12, 22] which consist of a nonlinear partial differential equation (PDE) and two ODEs. There are three types of Hopf bifurcations that can exist in the viscous MG equations corresponding to physical oscillations dominated by the ODE (surge), PDE (rotating stall), or a mixture of both. The objective of this particular work is to use optimization and regression techniques from machine learning to arrive at a lower dimensional description of the PDE from datasets. The success of compressor reduced-order modelling is rooted on accurate representations of the multi-physics and multi-fidelity models.

First, we describe the viscous MG equations, provide an explicit expression for the system's equilibrium, and show that the steady operating axial flow and pressure drifts from the aforementioned equilibrium during PDE bifurcation. Then, we introduce reduced-order modeling (ROM) to significantly alleviate computational costs by projecting the high dimensional state variables onto a low-dimensional subspace. We perform ROM on simulated data from viscous MG equations to construct a set of "good" basis functions. Approximations of bases spanning this subspace are constructed using principal component analysis (PCA) [15, 28] and both linear and nonlinear autoencoder neural networks [26, 27].

It is impossible to effectively "learn" from high dimensional data unless there is some kind of implicit or explicit low dimensional structure. Over the past 10 years, researchers have focused on sparsity as one type of criteria for low-dimensional structure. The inherent sparsity of natural signals is central to the mathematical framework of compressed sensing [5, 6, 9]. The main aim of compressed sensing is to construct a sparse vector from linear measurements of the vector such that the number of observed measurements m is significantly smaller than the dimension n of the original vector and satisfies the "Restricted Isometry Property" (RIP). Intuitively, the existence of a RIP implies that the geometry of sparse vectors is preserved through the measurement matrix, as illustrated in a high dimensional application [23]. These techniques rely heavily on the fact that many dynamical systems can be represented by governing equations that are sparse in the space of all possible functions. The assumption for the low dimensional structure for the MG equations originates from the center manifold theory in dynamical systems [13, 31], where a high dimensional system undergoing Hopf bifurcation can be fully described by projecting the equations onto the subspace of a 2-dimensional center manifold.

Finally, we adapt a recently developed technique called Sparse Identification of Nonlinear Dynamics (SINDy) [4, 7, 8] which has demonstrated the ability to recover governing equations of complex dynamical systems. The methods presented in SINDy approach the problem of automating the discovery of dynamic equations that describe natural systems through the lens of sparsity-promoting regression techniques such as Least Absolute Shrinkage and Selection Operator (LASSO) [29]. To lend insight into this process, the SINDy algorithm was applied to simulated data from various ROM models to recover their respective sparse equations which is then used to reconstruct the original system's dynamics.

Viscous Moore-Greitzer Equations

Model and Analysis

Turbo-jet engine is comprised of 3 parts: axial flow compressor where air gets compressed, the plenum where the air undergoes combustion and rapidly expands, and the turbine where the air is let out (see for example, Figure 1 in [30]). The flow enters from atmospheric pressure at the inlet duct, proceeds through the compressor block where the static pressure is increased, enters the outlet duct, and then exits to atmospheric pressure through the downstream turbine's throttle. The compressor is made out of an entrance duct, an inlet guide vane (IGV), multiple stages of stator-rotor pairs, and an exit duct towards the plenum. A stator is a rotary system with static blades and a rotor comprises of revolving blades.

The following basic assumptions of the MG compressor model [12, 22] are made. The pressure rise across the compressor lags behind the pressure drop delivered by the throttle due to mass storage in the exit duct (or plenum). Across the compressor, the difference between the pressure delivered by the compressor and pressure rise that currently exists across the compressor acts to accelerate the flow rate through the compressor. The flow is assumed to be incompressible and irrotational everywhere except inside the plenum where combustion occurs and rapidly expands the air.

The viscous MG equations for a cylindrical axial flow compressor consist of Laplace's partial differential equation (PDE) for disturbance velocity potential $\tilde{\phi}'(t,\theta,\eta)$

$$\tilde{\phi}'_{\eta\eta} + \tilde{\phi}'_{\theta\theta} = 0. \tag{1}$$

with boundary conditions

$$\psi_c(\Phi(t) + (\tilde{\phi}'_\eta)_0) - \frac{1}{2\pi}\int_0^{2\pi} \psi_c(\Phi(t) + (\tilde{\phi}'_\eta)_0)d\theta - m(\tilde{\phi}'_t)_0 - \frac{1}{a}(\tilde{\phi}'_{t\eta})_0 - \frac{1}{2a}(\tilde{\phi}'_{\eta\theta})_0 - \frac{\nu}{2a}(\tilde{\phi}'_{\eta\theta\theta})_0 = 0 \tag{2}$$

at $\eta = 0$ and $\tilde{\phi}' = 0$ at $\eta = -\infty$ and a pair of ordinary differential equations (ODEs) for annulus average of axial momentum $\Phi(t)$

$$\Psi(t) + \ell_c \frac{d\Phi(t)}{dt} = \frac{1}{2\pi}\int_0^{2\pi} \psi_c(\Phi(t) + (\tilde{\phi}'_\eta)_0)d\theta. \tag{3}$$

and pressure drop from across the compressor $\Psi(t)$

$$\frac{d\Psi(t)}{dt} = \frac{1}{4B^2\ell_c}(\Phi(t) - F_T^{-1}(\Psi(t))). \tag{4}$$

The subscripts of $\tilde{\phi}'$ indicate partial derivatives with respect to time t, angular θ and axial η coordinates of the cylindrical compressor. $(\cdot)_0$ means the quantity is evaluated at the compressor entrance $\eta = 0$. a is the internal compressor lag, $l_c = l_I + l_E + \frac{1}{a}$ is the characteristic compressor length (dimensionless quantity normalized with respect to compressor radius), and B is the plenum to compressor volume ratio [11]. Detailed derivation of the non-viscous model can be found in [11, 12, 22] while the viscous model was developed in [1, 21] and thoroughly derived in [3].

The compressor $\psi_c(\phi)$ and throttle $F_T(\phi)$ characteristic functions that are considered follow [12, 22]

$$\psi_c(\phi) = \psi_{c_0} + H\left[1 + \frac{3}{2}\left(\frac{\phi}{W} - 1\right) - \frac{1}{2}\left(\frac{\phi}{W} - 1\right)^3\right] \tag{5}$$

$$F_T(\phi) = \frac{\phi^2}{\gamma^2}. \tag{6}$$

H and W are the characteristic height and width of the compressor and ψ_{c_0} is a value determined by experiments. Throttle coefficient γ describes the amount of opening - large γ implies a wide open throttle while small γ implies a closed throttle. Equations (1), (2), (3), and (4) can be combined into a compact state-space form $\frac{\partial \mathbf{y}}{\partial t} = \mathbf{A}\mathbf{y} + \mathbf{f}(\mathbf{y})$ following [2]

$$\frac{\partial}{\partial t}\begin{bmatrix} g \\ \Phi \\ \Psi \end{bmatrix} = \begin{bmatrix} K^{-1}\left(\frac{\nu}{2}\frac{\partial^2}{\partial\theta^2} - \frac{1}{2}\frac{\partial}{\partial\theta}\right) & 0 & 0 \\ 0 & 0 & 0 \\ 0 & 0 & 0 \end{bmatrix}\begin{bmatrix} g \\ \Phi \\ \Psi \end{bmatrix} + \begin{bmatrix} aK^{-1}(\psi_c(\Phi+g) - \bar{\psi}_c) \\ \frac{1}{l_c}(\bar{\psi}_c - \Psi) \\ \frac{1}{4B^2 l_c}(\Phi - \gamma\sqrt{\Psi}) \end{bmatrix} \tag{7}$$

by introducing state variable g

$$g(t,\theta) = (\tilde{\phi}'_\eta)_0 = \sum_{n\in Z} |n|\tilde{\phi}'_n(t)e^{in\theta} = \sum_{n\in Z} g_n e^{in\theta}. \tag{8}$$

where

$$\tilde{\phi}'(t,\theta,\eta) = \sum_{n\in Z} \tilde{\tilde{\phi}}'_n(t)e^{|n|\eta + in\theta}, \tag{9}$$

is the solution to (1) and we define

$$\bar{\psi}_c = \frac{1}{2\pi}\int_0^{2\pi} \psi_c(\Phi + g)d\theta. \tag{10}$$

as well as an operator K that acts on $\phi = \sum_{n\in Z}\tilde{\phi}_n e^{in\theta}$ such that

$$K(\phi) = \sum_{n\in Z}\left(1 + \frac{ma}{|n|}\right)\tilde{\phi}_n e^{in\theta}. \tag{11}$$

To inspect the nonlinearities in $\mathbf{f}(\mathbf{y})$, we perform Taylor series' expansion on $\psi_c(\Phi + g)$ up to the third cubic term to expand the integrand of $\bar{\psi}_c$

$$\bar{\psi}_c = \psi_c(\Phi) + \frac{1}{2}\psi''_c(\Phi)\sum_{m,n\in Z}^{m+n=0} g_m g_n + \frac{1}{6}\psi'''_c(\Phi)\sum_{k,m,n\in Z}^{k+m+n=0} g_k g_m g_n. \tag{12}$$

Note that $g(t,\theta)$ has a vanishing average property due to assumptions made to the disturbance flow. Therefore, $\bar{\psi}_c$ is only a function of t and not θ and as a result, $K^{-1}(\bar{\psi}_c) = 0$. The nonlinearity vector $\mathbf{f}(\mathbf{y})$ becomes

$$\mathbf{f}(\mathbf{y}) = \begin{bmatrix} aK^{-1}(\psi_c'(\Phi)g + \frac{1}{2}\psi_c''(\Phi)g^2 + \frac{1}{6}\psi_c'''(\Phi)g^3) \\ \frac{1}{l_c}(\psi_c(\Phi) + \frac{1}{2}\psi_c''(\Phi)\sum_{m,n\in Z}^{m+n=0} g_m g_n + \frac{1}{6}\psi_c'''(\Phi)\sum_{k,m,n\in Z}^{k+m+n=0} g_k g_m g_n - \Psi) \\ \frac{1}{4B^2 l_c}(\Phi - \gamma\sqrt{\Psi}) \end{bmatrix}. \tag{13}$$

The system (7)'s equilibrium consist of $g_e(\theta) = 0$ and $\Psi_e = \psi_c(\Phi_e) = F_T(\Phi_e)$ which means (Φ_e, Ψ_e) lies on the intersection of curves (5) and (6). Φ_e can be solved by finding the root of the polynomial

$$-\frac{H}{2W^3}\Phi_e^3 + \left(\frac{3H}{2W^2} - \frac{1}{\gamma^2}\right)\Phi_e^2 + \psi_{c_0} = 0. \tag{14}$$

(14) has one real root and a pair of imaginary roots, where the real root is

$$\Phi_e = \sqrt[3]{X - Y^3 + \sqrt{X(X-2Y^3)}} + \sqrt[3]{X - Y^3 - \sqrt{X(X-2Y^3)}} - Y \tag{15}$$

and

$$X = \frac{W^3}{H}\psi_{c_0}, \qquad Y = \frac{2W^3}{3H}\left(\frac{1}{\gamma^2} - \frac{3H}{2W^2}\right). \tag{16}$$

For our analysis, γ is the bifurcation parameter to be varied for different kinds of Hopf bifurcation.

The Jacobian of $\mathbf{f}(\mathbf{y})$ at equilibrium is

$$\nabla\mathbf{f}_{\mathbf{y}_e} = \begin{bmatrix} aK^{-1}(\psi_c'(\Phi_e)) & 0 & 0 \\ 0 & \frac{1}{l_c}\psi_c'(\Phi_e) & -\frac{1}{l_c} \\ 0 & \frac{1}{4B^2 l_c} & -\frac{1}{4B^2 l_c}\frac{\gamma^2}{2\Phi_e} \end{bmatrix}. \tag{17}$$

The eigenvalues of $(\mathbf{A} + \nabla\mathbf{f}_{\mathbf{y}_e})$ corresponding to the PDE are

$$\lambda_n = \left(\frac{a|n|}{|n| + am}\right)\left(\psi_c'(\Phi_e) - \frac{\nu}{2a}n^2 - \frac{1}{2a}(in)\right) \tag{18}$$

and the eigenvalues of $(\mathbf{A} + \nabla\mathbf{f}_{\mathbf{y}_e})$ corresponding to the ODEs are

$$\mu_{1,2} = \frac{1}{2l_c}\left[\left(\psi_c'(\Phi_e) - \frac{\gamma}{8B^2\sqrt{\Psi_e}}\right) \pm \sqrt{\left(\psi_c'(\Phi_e) + \frac{\gamma}{8B^2\sqrt{\Psi_e}}\right)^2 - \frac{1}{B^2}}\right]. \tag{19}$$

Hopf bifurcation occurs when a pair of $(\mathbf{A} + \nabla\mathbf{f}_{\mathbf{y}_e})$ eigenvalues' real parts cross the imaginary axis with the derivative of the real parts with respect to γ is not equal to zero. There are three possibilities: surge (ODE bifurcation), stall (PDE bifurcation), and combination (simultaneous ODE and PDE bifurcations).

The critical bifurcation point for surge is $\gamma_{c,surge}$ such that $Re(\mu_{1,2}) = 0$. When $\gamma < \gamma_{c,surge}$, surge occurs. It is difficult to obtain an explicit expression for $\gamma_{c,surge}$ but $\gamma_{c,surge}$ is the solution to

$$\Phi_e(\gamma_{c,surge})\left(2 - \frac{\Phi_e(\gamma_{c,surge})}{W}\right) - \frac{\gamma_{c,surge}^2}{4B^2}\frac{W^2}{3H} = 0. \tag{20}$$

The condition for surge is $\frac{\partial}{\partial\gamma}(Re(\mu_{1,2}))\Big|_{\gamma_{c,surge}} > 0$.

The critical bifurcation point for stall is $\gamma_{c,stall}$ such that $Re(\lambda_1) = 0$. When $\gamma < \gamma_{c,stall}$, stall occurs. Again, it is difficult to obtain an explicit expression for $\gamma_{c,stall}$ but $\gamma_{c,stall}$ is the solution to

$$\Phi_e(\gamma_{c,stall})\left(2 - \frac{\Phi_e(\gamma_{c,stall})}{W}\right) - \frac{\nu W^2}{3aH} = 0. \tag{21}$$

The condition for stall is $\frac{\partial}{\partial\gamma}(Re(\lambda_1))\Big|_{\gamma_{c,stall}} > 0$.

It is possible for the largest PDE eigenvalue pairs and both ODE eigenvalues to simultaneously cross the imaginary axis. This is achieved when $\gamma = \gamma_{c,combo}$ where

$$\psi_c'(\Phi_e(\gamma_{c,combo})) = \frac{\gamma_{c,combo}^2}{8B^2}\frac{1}{\Phi_e(\gamma_{c,combo})} = \frac{\nu}{2a}. \tag{22}$$

For the combination case, it is possible to calculate the expression for the normal form which are the diagonal entries of $(\mathbf{A}+\nabla\mathbf{f}_{\mathbf{y}_e})(\gamma_{c,combo})$

$$\mathbf{D}(\gamma_{c,combo}) = \mathbf{T}^{-1}(\mathbf{A}+\nabla\mathbf{f}_{\mathbf{y}_e})\mathbf{T}(\gamma_{c,combo}) = \operatorname{diag}\left(\begin{bmatrix} (K^{-1}\left(\frac{\nu}{2}(1-n^2)-\frac{1}{2}ni\right) \\ \frac{1}{2l_c}\sqrt{\frac{\nu^2}{a^2}-\frac{1}{B^2}} \\ -\frac{1}{2l_c}\sqrt{\frac{\nu^2}{a^2}-\frac{1}{B^2}} \end{bmatrix}\right). \tag{23}$$

Rotating Stall Simulation Results

The system of equations (7) is integrated using the spectral method. $\theta \in [-\pi, \pi)$ is discretized into 512 equally spaced points, leading to a system of 514 ODEs (512 of which are Fourier coefficients of $g(t,\theta)$) to be numerically integrated using SciPy's `solve_ivp` with $dt = 0.1$. The following parameter values are used in all cases

$$l_c = 8, \quad m = 1.75, \quad a = 1/3.5, \quad \nu = 1, \quad \psi_{c_0} = 1.67H, \quad H = 0.18, \quad W = 0.25. \tag{24}$$

The plenum to compressor volume ratio B and the throttle opening γ are chosen to produce different type of bifurcations, and for the stall case, the simulations results are given below in Figure 1.

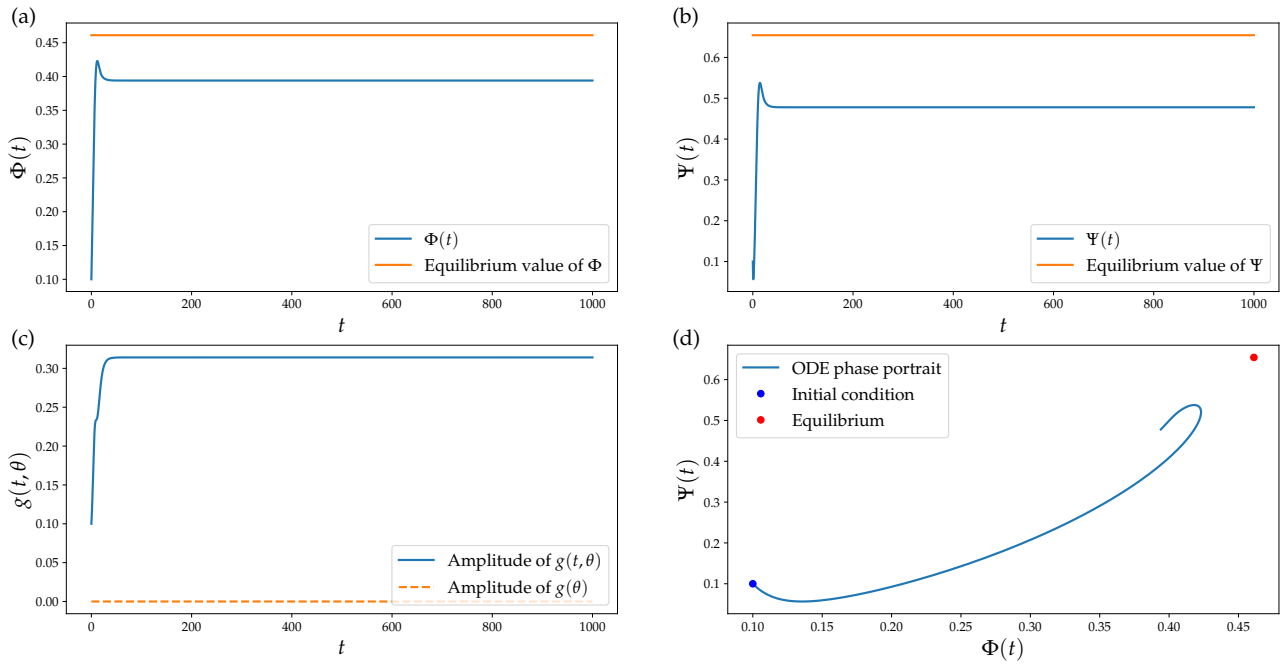

Figure 1: Stall dynamics of viscous Moore-Greitzer equations: (a) $\Phi(t)$ and (b) $\Psi(t)$ do not settle at their stable equilibrium values due to influence from PDE Hopf bifurcation. (c) Amplitude of $g(t,\theta)$ in t settles to a non-zero value during Hopf bifurcation. (d) Phase portrait of ODE states $\Phi(t)$ and $\Psi(t)$ which does not settle at the equilibrium point.

Dimensionality Reduction for Reduced-Order Modelling (ROM)

Principal Component Analysis (PCA)

PCA is also known as proper orthogonal decomposition (POD) in mechanical engineering [15] and discrete Karhunen-Loève expansion in signal processing and information theory [20]. PCA is a method to find principal axes in high dimensional data. These principal axes span the eigenvectors of the covariance matrix of the measurements which are orthonormal to each other such that the individual data along these directions are linearly uncorrelated. PCA can also be used as a dimensionality reduction tool by truncating a measurement's linear combination in its principal axes. Constructing basis functions from data using PCA can be formulated mathematically as a low-rank matrix approximation problem which can be easily computed by using the singular value decomposition (SVD) [10].

Suppose we have N observations of n-dimensional data

$$\mathbf{Y} = [\mathbf{y}_1 \dots \mathbf{y}_N] \tag{25}$$

where $\mathbf{Y} \in \mathbb{R}^{n\times N}$, $\mathbf{y_i} = \mathbf{y}(t_i) \in \mathbb{R}^n$. After centering the data about its empirical mean to get $\mathbf{Y}_0$, define a transformation $\mathbf{W} \in \mathbb{R}^{n\times m}$ where $m < n$ in the context of dimensionality reduction. The lower dimensional data is calculated by

$$\mathbf{X}_0 = \mathbf{W}^T \mathbf{Y}_0. \tag{26}$$

If we use PCA, then the transformation is defined as

$$\mathbf{W} = \mathbf{P}_m = [\mathbf{p}_1 \dots \mathbf{p}_m] \tag{27}$$

where $\mathbf{p}_m$ are the principal axes of $\mathbf{Y}_0$ or the first m eigenvectors of the covariance matrix $\mathbf{Y}_0\mathbf{Y}_0^T$.

Neural Network Implementation of PCA

An autoencoder is a type of multilayer feedforward neural network that at its simplest form (see Figure 2 without 64-nodes hidden layers) has an input layer with n nodes, followed by a hidden layer with m nodes (where $m < n$), followed by an output layer with n nodes. When the activation functions are chosen to be linear, the input-output relationship is given by

$$\hat{\mathbf{y}} = \mathbf{W}_2(\mathbf{W}_1\mathbf{y} + \mathbf{b}_1) + \mathbf{b}_2 \tag{28}$$

where $\mathbf{W}_1, \mathbf{W}_2^T \in \mathbb{R}^{m\times n}$ are the encoder and decoder weight matrices, and $\mathbf{b}_1 \in \mathbb{R}^m$, $\mathbf{b}_2 \in \mathbb{R}^n$ are the encoder and decoder bias vectors. Once the optimal $\{\mathbf{W}_1, \mathbf{W}_2, \mathbf{b}_1, \mathbf{b}_2\}$ are found, we can construct an encoder to reduce the input into a reduced-order data $\mathbf{x} \in \mathbb{R}^m$ using $\{\mathbf{W}_1, \mathbf{b}_1\}$ and a decoder to convert the encoded data back to its original dimension using $\{\mathbf{W}_2, \mathbf{b}_2\}$.

Under certain assumptions on the error function landscape, the minimization problem for the autoencoder reduces to

$$\min_{\{\mathbf{W}_2\}} \|\mathbf{Y}_0 - \mathbf{W}_2\mathbf{W}_2^+\mathbf{Y}_0\|_F^2. \tag{29}$$

where $\mathbf{W}_2^+$ is the Moore-Penrose inverse/pseudoinverse [25] of $\mathbf{W}_2$. For the case when the columns of $\mathbf{W}_2$ are orthonormal like $\mathbf{P}_m$, then $\mathbf{W}_2^+ = \mathbf{W}_2^T$ will make (29) equal to the reconstruction error of PCA. Therefore, it is clear that $\mathbf{P}_m$ is a solution to the autoencoder optimization problem. The problem is that the product of $\mathbf{P}_m$ with any proper orthogonal matrix $\mathbf{Q} \in \mathbb{R}^{m\times m}$ will be a minimizer $\mathbf{W}_2$, such that there are infinitely many solutions. Coupled with the fact that mini-batch stochastic gradient descent [19] is the go-to optimization algorithm in today's neural network frameworks, there is no guarantee that $\mathbf{W}_2$ converges to the same value when the training procedure is repeated, let alone align itself to $\mathbf{P}_m$. While any $\mathbf{W}_2$ in this space can be used to mimic the input data almost perfectly, this inconsistency is an issue in our problem as we would like to further uncover the underlying structure of the encoded measurements $\mathbf{X} = [\mathbf{x}_1 \dots \mathbf{x}_N]$.

Regularized Linear Autoencoder

An approach to recover the principal axes from autoencoder weights is based on the following hypothesis [26]: the first m left singular vectors of $\mathbf{W}$ is also the first m principal axes of $\mathbf{Y}_0$. This hypothesis can be framed as an autoencoder with a regularizer or penalty to the sum of the Frobenius norms of the encoder weight matrix $\mathbf{W}_1$ and decoder weight matrix $\mathbf{W}_2$

$$\min_{\{\mathbf{W}_1,\mathbf{W}_2\}} \|\mathbf{Y}_0 - \mathbf{W}_2\mathbf{W}_1\mathbf{Y}_0\|_F^2 + \lambda(\|\mathbf{W}_1\|_F^2 + \|\mathbf{W}_2\|_F^2). \tag{30}$$

For a large enough λ value, the error surface is guaranteed to be convex with a single global minima which will correspond to the principal axes [17]. Additionally, the minimum values of this loss function is $\mathbf{W}_1^* = \mathbf{W}_2^T$ unlike $\mathbf{W}_1^* = \mathbf{W}_2^+$ in the original approach.

Nonlinear Principal Component Analysis (NLPCA) and Autoencoder

NLPCA was developed to uncover the underlying nonlinear manifold in large dimensional datasets. The neural network architecture we are considering to train our NLPCA autoencoder is shown in Figure 2.

$$\begin{aligned} \mathbf{X} &= \mathbf{W}_2 \tanh(\mathbf{W}_1\mathbf{Y} + \mathbf{b}_1) + \mathbf{b}_2 \\ \hat{\mathbf{Y}} &= \mathbf{W}_4 \tanh(\mathbf{W}_3\mathbf{X} + \mathbf{b}_3) + \mathbf{b}_4. \end{aligned} \tag{31}$$

We choose the nonlinear activation function $\tanh()$ as in [27] under the justification that a trigonometric function would fit well with the solutions of the MG equations which are spanned by the Fourier basis (8). The NLPCA autoencoder is trained to minimize the loss function of

$$\min_{\{\mathbf{W}_{1,2,3,4},\mathbf{b}_{1,2,3,4}\}} \|\mathbf{Y} - \hat{\mathbf{Y}}\|_F^2. \tag{32}$$

The resulting $\{\mathbf{W}_{1,2,3,4}\}$ and $\{\mathbf{b}_{1,2,3,4}\}$ are then used to construct an encoder and decoder as per (31).

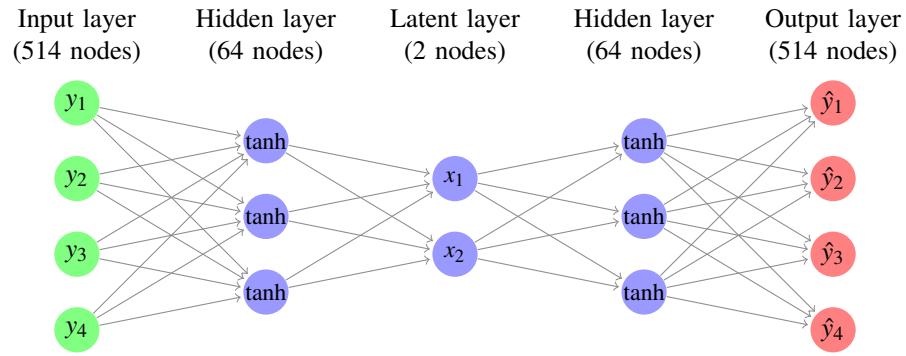

Figure 2: Autoencoder architecture for MG compressor data with tanh() activation function

Sparsity in Reduced-Order Data

Over the past two decades, researchers have focused on sparsity as one type of low-dimensional structure. Given the recent advances in both compressed sensing [6, 9] and sparse regression [29], it has become computationally feasible to extract system dynamics from large multimodal datasets. The term sparse in signal processing context refers to the case where signals (or any type of data, in general) have few non-zero components with respect to the total number of components. It is well known in dynamical systems, the normal forms provide a way of finding a coordinate system in which the dynamical system takes the "simplest" or "minimal" form. The normal forms, which are sparse in the space of homogeneous vector polynomial of certain degree, is calculated by making judicious choices of the solutions to the homological equations [13]. Hence, in the context of our work, close to the bifurcation point, the sparse regression techniques rely heavily on the fact that many dynamical systems can be represented by governing equations that are sparse in the space of all possible functions of a given algebraic structure.

Compressed Sensing

Compressed sensing (CS) is a technique for sampling and reconstructing sparse signals that can be represented by $k << n$ significant coefficients over an n- dimensional basis. The central goal of CS is the recovery of sparse vectors from a small number of linear measurements, which distinguishes CS from other dimensionality reduction techniques. In [9] and [6], the original sparse (k-sparse) signal is projected onto a lower-dimensional subspace via a random projection scheme, called the sampling matrix. More precisely, this broader objective is exemplified by the important special case in which one is interested in finding a vector $S \in \mathbb{R}^n$ using the (noisy) observation or the measurement data

$$Y = \Theta S + \eta, \quad \text{where } \Theta \in \mathbb{R}^{m \times n} \text{ with } k < m < n, \tag{33}$$

is the known sensing or sampling matrix and η is the measurement noise.

In general, this problem cannot be solved uniquely. However, if S is k-sparse i.e., if it has up to k non-zero entries, the theory of CS shows that it is possible to reconstruct S, a k-sparse vector in $\mathbb{R}^n$ uniquely from m linear measurements even when $m << n$, by exploiting the sparsity of S. This can be achieved by finding the sparsest signal consistent with the vector of measurements [9], i.e.

$$\underset{S \in \mathbb{R}^n}{\arg\min} \|S\|_0 \text{ subject to } \|Y - \Theta S\|_2 \leq \varepsilon \tag{34}$$

where $\|S\|_0$ denotes the l_0 norm for S (the number of non-zero entries of S), while ε denotes a parameter that depends on the level of measurement noise η. However, l_0 minimization problem (34) is a non-convex problem which is NP-hard.

Instead of problem (34) we consider its l_1 convex relaxation which may be stated as

$$\underset{S \in \mathbb{R}^n}{\arg\min} \|S\|_1 \text{ subject to } \|Y - \Theta S\|_2 \leq \varepsilon \tag{35}$$

where the l_1 norm (sum of the absolute values of the entries of S) is a convex function. Hence (35) is a convex optimization problem which can accurately approximate the solution to (34) in polynomial time with high probability if measurement matrix Θ is chosen to satisfy a necessary condition called "Restricted Isometry Property" (RIP) [5, 6]. One should note that the l_1 minimization in (35) is closely related to the LASSO problem [29]

$$\underset{S \in \mathbb{R}^n}{\arg\min} \|Y - \Theta S\|_2^2 + \alpha \|S\|_1 \tag{36}$$

where $\alpha \geq 0$ is a regularization parameter. If ε and α in (35) and (36) satisfy some special conditions, the two problems are equivalent; however, characterizing the relationships between ε and α is difficult except for the special case of orthogonal sensing matrices Θ. The practical success of the LASSO can be attributed to the fact that in many cases S is sparse.

Sparse Identification of Dynamical Systems (SINDy)

Sparse identification of nonlinear dynamics (SINDy) [4] is an algorithm for discovering the dynamical equations directly from the data. The problem of model discovery from data can be formulated as a feature selection problem in machine learning. The SINDy algorithm takes m-time measurements of $\mathbf{x} \in \mathbb{R}^n$, $\mathbf{X} = [\mathbf{x}(t_1), \ldots, \mathbf{x}(t_m)]^T \in \mathbb{R}^{m \times n}$ and attempts to discover the structure of a nonlinear differential equation of the form

$$\dot{\mathbf{X}} = \mathbf{f}(\mathbf{X}(t)) \approx \Theta(\mathbf{X})\mathbf{S} \tag{37}$$

where $\Theta(\mathbf{X}) = [\theta_1(\mathbf{X}), \theta_2(\mathbf{X}), ..., \theta_p(\mathbf{X})] \in \mathbb{R}^{m \times p}$ form the dictionary of basis functions, and $\mathbf{S} = [\mathbf{s}_1 \ ... \ \mathbf{s}_k \ ... \ \mathbf{s}_n] \in \mathbb{R}^{p \times n}$ is the matrix of coefficients, where each column $\mathbf{s}_k$ corresponds to an equation with p terms. p is the maximal number of n-multivariate monomials of degree at most d. The majority of $\mathbf{S}$ entries are zero while the remaining non-zero entries identify the active terms contributing to the sparse representation of the dynamics $\mathbf{f}(\mathbf{X})$. To guarantee sparsity, SINDy is reformulated as a LASSO problem

$$\arg\min_{\mathbf{s}_k} \frac{1}{m} \sum_{i=1}^{m} \|\dot{\mathbf{x}}(t_i) - \Theta(\mathbf{x}(t_i))\mathbf{s}_k\|_2^2 + \alpha \|\mathbf{s}_k\|_1 \tag{38}$$

where α is the l_1 regularization coefficient. LASSO is an optimization algorithm that finds a sparse solution for (38) by initializing $\mathbf{s}_k = \mathbf{0}$ and at each iteration, it tries to find an update for $\mathbf{s}_k$ one entry at a time. The coefficient α acts as a threshold such that if the an optimal condition involving α is not satisfied for a particular $\mathbf{s}_k$ entry, the entry is chosen to be equal to zero. Increasing the value of α leads to more zero entries in $\mathbf{s}_k$, resulting in a sparse model.

The dictionary of basis functions for monomial sampling of dynamical system is

$$\Theta(\mathbf{X}) = \begin{bmatrix} | & | & | & | & | \\ \mathbf{1} & \mathbf{X} & \mathbf{X^{P_2}} & \mathbf{X^{P_3}} & \ldots \\ | & | & | & | & | \end{bmatrix}. \tag{39}$$

The dictionary $\Theta(\mathbf{X})$ is constructed by appending candidate nonlinear functions of $\mathbf{X}$ column-wise. Here, higher order polynomials are denoted as $\mathbf{X}^{P_d}$ where d is the order of the polynomial considered. For example, element 1 is a column-vector of ones, element $\mathbf{X}$ is as defined above, element $\mathbf{X}^{P_2}$ is the matrix containing the set of all quadratic polynomial functions of the state vector $\mathbf{x}$, and is constructed as follows:

$$\mathbf{X^{P_2}} = \begin{bmatrix} x_1^2(t_1) & x_1(t_1)x_2(t_1) & \ldots & x_2^2(t_1) & \ldots & x_n^2(t_1) \\ x_1^2(t_2) & x_1(t_2)x_2(t_2) & \ldots & x_2^2(t_2) & \ldots & x_n^2(t_2) \\ \vdots & \vdots & \ddots & \vdots & \ddots & \vdots \\ x_1^2(t_m) & x_1(t_m)x_2(t_m) & \ldots & x_2^m(t_m) & \ldots & x_n^2(t_m) \end{bmatrix}. \tag{40}$$

We interpolate the reduced MG simulation data as a dynamical systems with cubic nonlinearity which is up to $\mathbf{X^{P_3}}$.

ROM Results and Analysis

We run 10 simulations of the viscous MG equations' stall case for $t \in [0, 500]$ with $dt = 0.1$. The initial conditions for $g(t, \theta)$'s amplitude, Φ, and Ψ are drawn from the normal distribution with mean 0.1 and standard deviation 0.05. The first 2000 data points (up to $t = 200$) containing the transient dynamics are discarded. This gives us 10 $\mathbf{Y} \in \mathbb{R}^{3000 \times 514}$ datasets. We perform k-fold cross validation [14] on PCA, regularized autoencoder, and NLPCA autoencoder to find the best ROM parameters to bring down the data dimension to 2. Both autoencoders' training were performed using Adam optimizer [16] with learning rate of 10^{-4} for 10 epochs of 4 mini-batch size for the regularized linear autoencoder and 20 epochs of 4 mini-batch size for the NLPCA autoencoder.

We encode the 10 datasets using the 3 different encoders to obtain 3 versions of 10 $\mathbf{X} \in \mathbb{R}^{3000 \times 2}$. For each group of reduced-order/encoded data, we perform a cubic nonlinearity dynamical system identification using PySINDy [8] paired with LASSO optimizer from Python's `sklearn` package. We train the 3 groups of 10 $\mathbf{X}$ datasets in order to find the best α which hits the sweet spot between sparsity and accuracy using grid search [18]. After finding the best α for each group, we perform another k-fold cross validation to decide on a model that best represent the 10 datasets of each ROM.

The discovered reduced governing equations satisfy the normal form if it is sufficiently described by 4 coefficients μ, ω, b_1, b_2 up to an acceptable numerical tolerance

$$\begin{aligned} \dot{x}_1 &= \mu x_1 - \omega x_2 + b_1(x_1^2 + x_2^2)x_1 - b_2(x_1^2 + x_2^2)x_2 \\ \dot{x}_2 &= \omega x_1 + \mu x_2 + b_2(x_1^2 + x_2^2)x_1 + b_1(x_1^2 + x_2^2)x_2. \end{aligned} \tag{41}$$

However, when the linear operator is semi-simple (as in Hopf bifurcations), the correct identification of a normal form depends critically on the null space of the homological operator [13]. The consequence of this fact is that the nonlinear terms in normal form (41) commutes with the linear term. As shown in [24], a consequence of this property is that, when the equation is normalized to any finite degree, say $k = 3$, and truncated, it will have symmetries that were not present in the original system. More precisely, rewriting the normal form equations (41) at the bifurcation point ($\mu = 0$) as

$$\dot{\mathbf{x}} \quad = \quad A\mathbf{x} + f^*(\mathbf{x}) \quad \mathbf{x} \in \mathbb{R}^2, \tag{42}$$

and letting $\mathbf{x} = \exp(At)\mathbf{y}$, the transformed equations are

$$\dot{\mathbf{y}} \quad = \quad \exp(-At) f^*(\exp(At)\mathbf{y}) \quad \mathbf{y} \in \mathbb{R}^2. \tag{43}$$

Using the commutation property [24] of the normal form f^*,

$$\exp(-At) f^*(\exp(At)\mathbf{y}) = f^*(\mathbf{y}), \quad \forall t \in \mathbb{R},\ \forall \mathbf{y} \in \mathbb{R}^2,$$

the normal form equations in the new variables $\mathbf{y}$ reduce to

$$\dot{\mathbf{y}} \quad = \quad f^*(\mathbf{y}) \quad \mathbf{y} \in \mathbb{R}^2. \tag{44}$$

For post-bifurcation dynamics, the discovered reduced governing equations satisfy the normal form (44) if it is sufficiently described by 2 coefficients (b_1, b_2) up to an acceptable tolerance

$$\begin{aligned} \dot{y}_1 &= b_1(y_1^2 + y_2^2)y_1 - b_2(y_1^2 + y_2^2)y_2 \\ \dot{y}_2 &= b_2(y_1^2 + y_2^2)y_1 + b_1(y_1^2 + y_2^2)y_2. \end{aligned} \tag{45}$$

Hence, MG equations close to a Hopf bifurcation have a sparse representation (45) with respect to high-dimensional polynomial spaces. The practical success and importance of the LASSO can be attributed to correctly identifying the relevant variables when the underlying model is sparse. LASSO algorithm is used in the subsequent sections to recover a system of two sparse ordinary differential equations (ODEs) with cubic nonlinearities.

For the reconstruction, the obtained SINDy equations are integrated using the forward Euler method with a fixed integration time step $dt = 0.1$ to be consistent with the chosen smoothed forward difference differentiation scheme. The global truncation error is then subtracted from the raw numerical integration result to correct the estimate. Lastly, the integrated SINDy data are fed into the decoder of the respective reduction methods to reconstruct the high dimensional time series and compared with the original dataset.

PCA and SINDy

The best SINDy regression is obtained using a LASSO threshold of $\alpha = 0.11$, which outputs a system of two ODEs with 8 coefficients and a R^2 score of 0.9999 on the test data $|||\dot{\mathbf{X}}|||$ as

$$\begin{aligned} \dot{x}_1 &= -0.000144x_1^3 - 0.008137x_1^2x_2 - 0.000144x_1x_2^2 - 0.008136x_2^3 \\ \dot{x}_2 &= 0.008136x_1^3 - 0.000144x_1^2x_2 + 0.008136x_1x_2^2 - 0.000144x_2^3. \end{aligned} \tag{46}$$

The normal form coefficients $(-0.000144, 0.008136)$ are visibly detected. Reconstruction results for a chosen random dataset are shown on the left in Figure 3.

Regularized Linear Autoencoder and SINDy

The best SINDy regression is obtained using a LASSO threshold of $\alpha = 0.30$. The output is a system of two ODEs with 9 coefficients and a R^2 score of 0.9999 on the test data $|||\dot{\mathbf{X}}|||$ and is given as

$$\begin{aligned} \dot{x}_1 &= -0.000440x_2^2 - 0.000145x_1^3 + 0.008138x_1^2x_2 - 0.000143x_1x_2^2 + 0.008138x_2^3 \\ \dot{x}_2 &= -0.008136x_1^3 - 0.000144x_1^2x_2 - 0.008139x_1x_2^2 - 0.000144x_2^3. \end{aligned} \tag{47}$$

The normal form coefficients $(-0.000145, -0.008138)$ are also visibly detected, albeit with wider deviation in values compared to (46) and an additional quadratic term in the first equation. Reconstruction results for a chosen random dataset are shown on the right in Figure 3.

NLPCA Autoencoder and SINDy

The best SINDy regression is obtained using a LASSO threshold of $\alpha = 0.60$. The output is a system of two ODEs with 11 coefficients and a R^2 score of 0.9998 on the test data $|||\dot{\mathbf{X}}|||$ which does not satisfy the normal form. A representative equation (since the outcome is always random) is given as

$$\begin{aligned} \dot{x}_1 &= -0.001031x_2^2 - 0.000091x_1^3 + 0.007704x_1^2x_2 + 0.000429x_1x_2^2 + 0.006863x_2^3 \\ \dot{x}_2 &= -0.001664x_1^2 - 0.000580x_2^2 - 0.007607x_1^3 - 0.000473x_1^2x_2 - 0.007470x_1x_2^2 - 0.000237x_2^3. \end{aligned} \tag{48}$$

Reconstruction results for a chosen random dataset are shown in Figure 4.

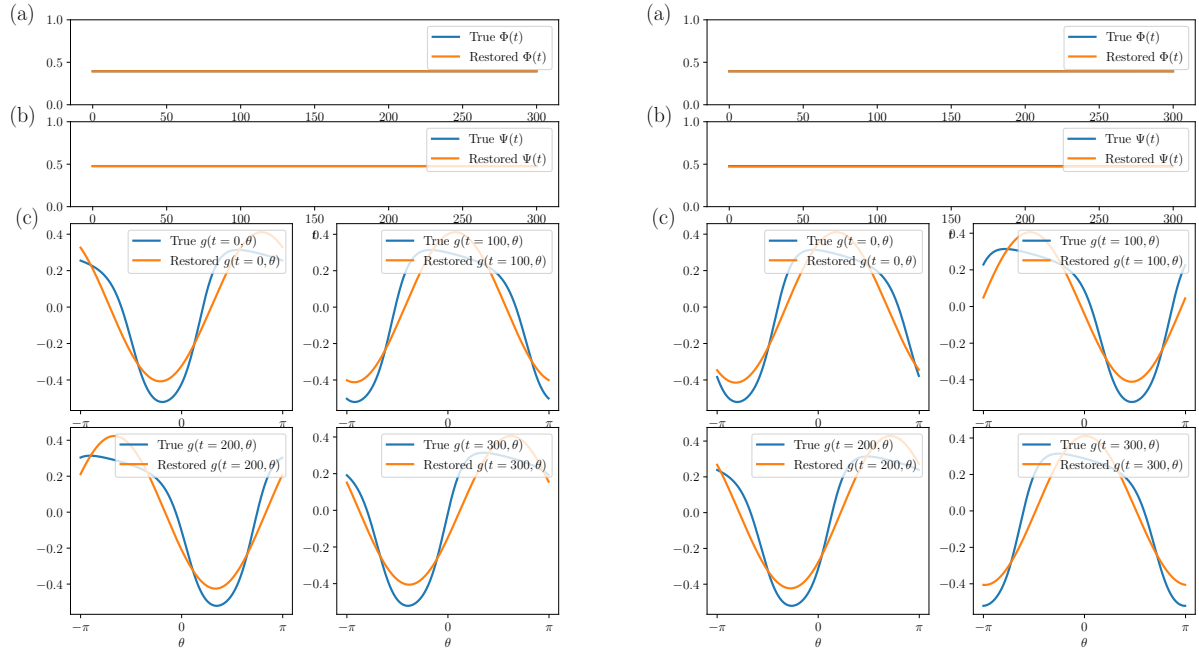

Figure 3: Reconstruction of viscous MG stall dynamics using PCA and SINDy (on the left) and regularized linear autoencoder and SINDy (on the right): (a) $\Phi(t)$, (b) $\Psi(t)$, and (c) $g(t,\theta)$ reconstruction results at $t = 0, 100, 200, 300$

Conclusions

We have showed that it is possible to fully reconstruct the solutions of the viscous MG equations from a system of 2 ODEs up to cubic nonlinearity, constructed from data sets by sparse regression. Additionally, it seems that the only requirement to detect the normal form of the PDE Hopf bifurcation is to have reduced-order data that falls along the first two principle axes, and reconstruction quality is entirely independent of whether normal forms of the underlying PDE is detected or not. The NLPCA autoencoder has to be trained for twice as long (double the number of epochs) compared to the linear autoencoder in order to converge to the local minimum that produces great reconstruction result. Table 1 summarizes our findings for the three chosen dimensionality reduction methods. Our simple approach rooted in physics-based machine learning which involves a priori knowledge of sparsity and the center manifold theory allows us to bypass deep neural network performing synchronized dimensionality reduction and SINDy approach in [7]. It is shown in Table 1 that performing dimensionality reduction and SINDy independently does not result in any significant reconstruction loss. Additionally, it would be interesting to find out if nonlinear principal components would lead us to normal form discovery from a nonlinear autoencoder, and if those components can be found using a simple regularization based approach to ensure the convexity of loss landscape just like its linear counterpart [17].

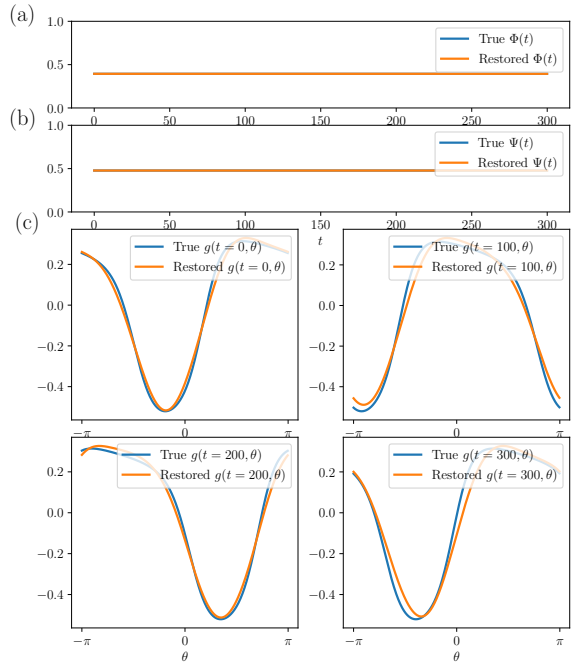

Figure 4: Reconstruction of viscous MG stall dynamics using NLPCA autoencoder and SINDy

	PCA	Linear Autoencoder	NLPCA Autoencoder
Training time	25 s	103 s	283 s
PDE reconstruction R^2 score from training data	0.8973	0.8973	0.9916
PDE reconstruction R^2 score from SINDy equations	0.8950	0.8948	0.9890
Number of RHS terms in reduced equations	8	9	11
Normal form detected	yes	yes	no

Table 1: Summary of viscous MG equations' reconstruction from SINDy models identified from different ROMs.

Acknowledgements: The authors acknowledge partial support for this work from NSERC Discovery grant 50503-10802, TECSIS /Fields-CQAM Lab for Inference and Prediction, and NSERC CRD grant 543433-19. The authors are also grateful to Mr. Yiming Meng his contribution in the viscous MG simulation development.

References

[1] Adomaitis, R. A., Abed, E. H. (1993) Local nonlinear control of stall inception in axial flow compressors. Proc. AIAA 29th Joint Propulsion Conference and Exhibit, 2230.

[2] Birnir, B., Hauksson H. A. (2000) Basic Control for the Viscous Moore–Greitzer Partial Differential Equation. SIAM J. Control Optim., 38(5), 1554-1580.

[3] Birnir, B., Hou, S., Wellander, N. (2007) Derivation of the viscous Moore-Greitzer equation for aeroengine flow. J. Math. Phys., 48(6), 065209-065209.

[4] Brunton, S. L., Proctor, J. L., Kutz, J. N. (2016) Discovering governing equations from data by sparse identification of nonlinear dynamical systems. Proc. Natl. Acad. Sci. U. S. A., 113(15), 3932-3937.

[5] Candés, E.J., Tao, T. (2005) Decoding by linear programming. IEEE Trans. Inf. Theory, 51(12), 4203-4215.

[6] Candés, E. J., Romberg, J. K., Tao, T. (2006) Stable signal recovery from incomplete and inaccurate measurements. Comm. Pure Appl. Math., 59(8), 1207-1223.

[7] Champion K., Lusch B., Kutz J. N., Brunton S. (2019) Data-driven discovery of coordinates and governing equations. Proc. Natl. Acad. Sci. U. S. A., 116(45), 22445-22451.

[8] de Silva, B., Champion, K., Quade, M., Loiseau, J. C., Kutz, J., Brunton, S. (2020) PySINDy: A Python package for the sparse identification of nonlinear dynamical systems from data. J. Open Sources Software, 5(49), 2104.

[9] Donoho D. L. (2006) Compressed sensing. IEEE Trans. Inform. Theory, 52(4), 1289-1306.

[10] Golub, G., Kahan, W. (1964) Calculating the Singular Values and Pseudo-Inverse of a Matrix. J. Soc. Ind. Appl. Math. B, 2(2), 205–224.

[11] Greitzer, E. M. (1976) Surge and rotating stall in axial flow compressors—Part I: Theoretical compression system model. J. Eng. Power, 98(2), 190-198.

[12] Greitzer, E. M., Moore, F. K. (1986) A theory of post-stall transients in axial compression systems: part II—application. Trans. ASME: J. Eng. Gas Turbines Power, 108(2), 231-239.

[13] Guckenheimer, J., Holmes, P. (1983) Nonlinear oscillations, dynamical systems, and bifurcations of vector fields. Springer-Verlag.

[14] Hastie, T., Tibshirani, R., Friedman, J. (2009) The elements of statistical learning: data mining, inference, and prediction. Springer Science & Business Media.

[15] Holmes, P., Lumley, J. L., Berkooz, G., Rowley, C. W. (2012) Turbulence, coherent structures, dynamical systems and symmetry. Cambridge University Press.

[16] Kingma, D.P., Ba, J. (2014) Adam: A Method for Stochastic Optimization. Proc. 3rd Intl. Conf. Learning Representations.

[17] Kunin D., Bloom J., Goeva A., Seed C. (2019) Loss Landscapes of Regularized Linear Autoencoders. Proc. 36th Intl. Conf. Machine Learning, 97, 3560-3569.

[18] Larochelle, H., Erhan, D., Courville, A., Bergstra, J., Bengio, Y. (2007) An empirical evaluation of deep architectures on problems with many factors of variation. Proc. 24th Intl. Conf. Machine Learning, 473-480.

[19] Li, M., Zhang, T., Chen, Y., Smola, A. J. (2014) Efficient mini-batch training for stochastic optimization. Proc. 20th ACM SIGKDD Intl. Conf. Knowledge Discovery and Data Mining, 661-670.

[20] Loève, M. (1978) Probability theory. Vol. II, 4th ed. Graduate Texts in Mathematics 46. Springer-Verlag.

[21] Mezić, I. (1998) A large-scale theory of axial compression system dynamics. Preprint.

[22] Moore, F. K., Greitzer, E. M. (1986) A theory of post-stall transients in axial compression systems: Part I—Development of equations. Trans. ASME: J. Eng. Gas Turbines Power, 108(1), 68-76.

[23] Mukherjee, A., Aydogdu, Y., Ravichandran, T., and Sri Namachchivaya, N. (2022) Stochastic Parameterization Using Compressed Sensing: Application to the Lorenz-96 Atmospheric Model. Tellus A: Dynamic Meteorology and Oceanography, 74(2022), pp.300–317.

[24] Namachchivaya, N. S., Doyle, M. M., Langford, W. F., Evans, N. W. (1994) Normal form for generalized Hopf bifurcation with non-semisimple 1:1 resonance. ZAMP, 45(2), 312-335.

[25] Penrose, R. (1955) A generalized inverse for matrices. Proc. Cambridge Philos. Soc., 51(3), 406–413.

[26] Plaut E. (2018) From Principal Subspaces to Principal Components with Linear Autoencoders. arXiv preprint, 1804.10253.

[27] Scholz M., Vigário R. (2002) Nonlinear PCA: a new hierarchical approach. Proc. ESANN, 439-444.

[28] Sirovich, L. (1987) Turbulence and the dynamics of coherent structures. I. Coherent structures. Q. Appl. Math., 45(3), 561-571.

[29] Tibshirani, R. (1996) Regression shrinkage and selection via the lasso. J. R. Stat. Soc. B, 58(1), 267-288.

[30] Xiao, M. (2008) Quantitative characteristic of rotating stall and surge for Moore–Greitzer PDE model of an axial flow compressor. SIAM J. Appl. Dyn. Syst., 7(1), 39-62.

[31] Xiao, M., Basar, T. (2000) Center manifold of the viscous Moore-Greitzer PDE model. SIAM J. Appl. Math., 61(3), 855–869.